Journal of Catalysis 276 (2010) 249–258

Contents lists available at ScienceDirect

Journal of Catalysis

journal homepage: www.elsevier.com/locate/jcat

# Hydrodesulfurization properties of rhodium phosphide: Comparison with rhodium metal and sulfide catalysts

John R. Hayes, Richard H. Bowker, Amy F. Gaudette, Mica C. Smith, Cameron E. Moak, Charles Y. Nam, Thomas K. Pratum, Mark E. Bussell *

*Department of Chemistry and Advanced Materials Science and Engineering Center, MS-9150, Western Washington University, Bellingham, WA 98225, United States*

ARTICLE INFO

*Article history:*
Received 3 September 2010
Revised 8 September 2010
Accepted 11 September 2010
Available online 28 October 2010

*Keywords:*
Hydrodesulfurization
HDS
Dibenzothiophene
Rhodium
Rhodium phosphide

ABSTRACT

Silica-supported rhodium phosphide ($Rh_2P/SiO_2$) catalysts were prepared and characterized by X-ray diffraction (XRD), transmission electron microscopy (TEM), $^{31}P$ solid-state NMR spectroscopy, X-ray photoelectron spectroscopy (XPS), and chemisorption measurements. XRD and TEM analysis of a 5 wt.% $Rh_2P/SiO_2$ catalyst confirmed the presence of well-dispersed $Rh_2P$ crystallites on the silica support having an average crystallite size of 10 nm. NMR spectroscopy showed unsupported and silica-supported $Rh_2P$ to be metallic and XPS spectroscopy yielded a surface composition of $Rh_{1.94}P_{1.00}$ that is similar to that expected from the bulk stoichiometry. The 5 wt.% $Rh_2P/SiO_2$ catalyst exhibited a higher dibenzothiophene (DBT) hydrodesulfurization (HDS) activity than did $Rh/SiO_2$ and sulfided $Rh/SiO_2$ catalysts having a similar Rh loading and was also more active than a commercial Ni—Mo/$Al_2O_3$ catalyst. The $Rh_2P/SiO_2$ catalyst showed excellent stability over a 100 h DBT HDS activity measurement and was more S tolerant than the $Rh/SiO_2$ catalyst. The $Rh_2P/SiO_2$ catalyst strongly favored the hydrogenation pathway for DBT HDS, while the $Rh/SiO_2$ and sulfided $Rh/SiO_2$ catalysts favored the direct desulfurization pathway.



## 1. Introduction

Among monometallic sulfides, rhodium sulfide ($Rh_2S_3$) has been observed to be one of the most active for the hydrodesulfurization (HDS) of the organosulfur compounds thiophene, dibenzothiophene (DBT), and 4,6-dimethyldibenzothiophene (4,6-DMDBT) [1–6]. Under the conditions of low hydrogen sulfide ($H_2S$) partial pressure, noble metals (including Rh) have been shown to be highly active for deep HDS applications [7–13]. As a result, noble metal catalysts are being investigated for use in second-stage HDS processing, where the $H_2S$ partial pressure can be kept low, for the production of low sulfur diesel.

A substantial body of literature has shown that metal phosphide catalysts have promising HDS properties [14]. Previous studies in our laboratory of monometallic and bimetallic phosphides indicate that these materials are both highly active for HDS and resistant to sulfur incorporation. For example, we recently reported that a 25 wt.% $Fe_{0.03}Ni_{1.97}P/SiO_2$ catalyst (P/Me = 1.0 in the oxidic precursor) was slightly more active (on a mass catalyst basis) than a commercial Co—Mo/$Al_2O_3$ catalyst for DBT HDS [15]. XRD and XPS measurements of HDS-tested $Fe_{0.03}Ni_{1.97}P/SiO_2$ catalysts indicated no loss of phase purity and a surface composition, $Fe_{0.12}Ni_{1.49}P_{1.00}S_{\leqslant 0.05}$, indicating no significant sulfur incorporation. It is of interest, therefore, to determine whether noble metal phosphides have the excellent HDS properties observed for noble metals (and noble metal sulfides), while also having the improved resistance to S poisoning observed for metal phosphide catalysts.

The synthesis of unsupported $Rh_2P$ via temperature-programmed reduction (TPR) of a metal phosphate precursor was recently reported in the literature [16], and this procedure was readily adapted for the synthesis of $Rh_2P/SiO_2$ catalysts. $Rh_2P$ adopts the anti-fluorite structure ($Fm\bar{3}m$ space group) in which the Rh atoms occupy tetrahedral positions and the P atoms occupy cubic positions in the lattice [17]; the $Rh_2P$ unit cell is shown in Fig. 1. While $Rh_2P$ is metallic, its catalytic properties are expected to be different from those of Rh metal (and Rh sulfide). In this study, the HDS properties of low loading rhodium phosphide (5 wt.% $Rh_2P/SiO_2$) catalysts were investigated and compared to those of rhodium sulfide (sulfided $Rh/SiO_2$) and rhodium metal ($Rh/SiO_2$) catalysts.

## 2. Experimental methods

### 2.1. Catalyst synthesis

Silica-supported rhodium phosphide ($Rh_2P/SiO_2$) catalysts were prepared with a 5 wt.% $Rh_2P$ loading using the following procedure.

* Corresponding author. Address: Department of Chemistry, MS-9150, Western Washington University, 516 High Street, Bellingham, WA 98225, United States. Fax: +360 650 2826.
*E-mail address:* Mark.Bussell@wwu.edu (M.E. Bussell).

0021-9517/$ - see front matter © 2010 Elsevier Inc. All rights reserved.
doi:10.1016/j.jcat.2010.09.013

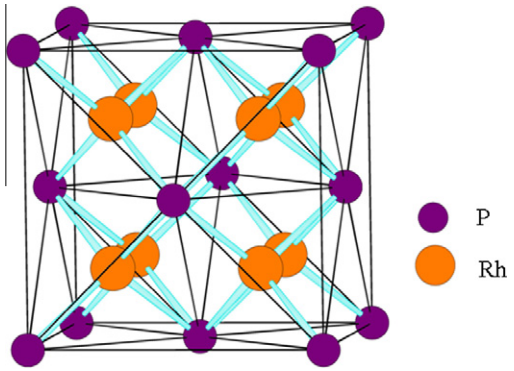


**Fig. 1.** Structural model of the $Rh_2P$ unit cell.

A precursor composition having an excess of P (P/Rh = 0.75) was used. A solution of 0.188 g $RhCl_3{\cdot}xH_2O$ ($x \approx 2.9$, Johnson Matthey, 99.9%) and 0.0578 g $NH_4H_2PO_4$ (Alfa Aesar, 98.0%) in nanopure water was impregnated onto 1.50 g $SiO_2$ (Cab-O-Sil, M-7D grade, 200 $m^2/g$) to incipient wetness, followed by drying of the impregnated support at 383 K. Multiple impregnations were necessary to transfer all the solution onto the silica. Following the final impregnation, the impregnated support was dried for 24 h, then calcined at 773 K for 3 h in air. The resulting solid was ground to a fine powder and then reduced in a 300 mL/min $H_2$ (Airgas, 99.999%) flow, while the temperature was increased from room temperature to 923 K at a rate of 1 K/min. Following cooling to room temperature in continued $H_2$ flow, the $Rh_2P/SiO_2$ catalyst was subjected to a 60 mL/min He flow for 30 min followed by passivation in a 1.0 mol% $O_2$/He (Airgas) mixture at 30 mL/min for 2 h. Unsupported $Rh_2P$ and a 25 wt.% $Rh_2P/SiO_2$ catalyst, used in some of the characterization measurements, were synthesized similarly except that the precursor for the unsupported $Rh_2P$ was prepared by evaporating a solution of $RhCl_3{\cdot}xH_2O$ and $NH_4H_2PO_4$ salts.

A precursor of silica-supported Rh metal ($Rh/SiO_2$) and Rh sulfide (sulfided $Rh/SiO_2$) catalysts with an Rh loading equivalent to that of the 5 wt.% $Rh_2P/SiO_2$ catalyst (4.4 wt.% Rh) was prepared as follows. A solution of 0.188 g $RhCl_3{\cdot}xH_2O$ ($x \approx 2.9$, Johnson Matthey, 99.9%) in nanopure water was impregnated onto 1.50 g $SiO_2$ (Cab-O-Sil, M-7D grade, 200 $m^2/g$) to incipient wetness, followed by drying of the impregnated support at 383 K. Multiple impregnations were necessary to transfer all the solution onto the silica. Following the final impregnation, the impregnated support was dried for 24 h, then calcined at 773 K for 3 h in air.

### 2.2. Catalyst characterization

X-ray diffraction (XRD) patterns of the catalysts were obtained using a PANalytical X'Pert Pro diffractometer equipped with a monochromatic Cu Kα source ($\lambda$ = 1.54050 Å). Approximately 0.020 g of catalyst was mixed with a small amount of acetone, and the mixture was deposited onto a microscope slide. Following evaporation of the acetone, the microscope slide was mounted on the sample stage for XRD pattern acquisition. Transmission electron microscopy (TEM) measurements were obtained with a JEOL 2010 high-resolution transmission electron microscope operating at 200 keV. A sample of a 5 wt.% $Rh_2P/SiO_2$ catalyst was placed on a 200 mesh copper grid coated with formvar and carbon.

Solid-state $^{31}P$ nuclear magnetic resonance (NMR) spectra of unsupported $Rh_2P$ and 5 and 25 wt.% $Rh_2P/SiO_2$ catalysts were obtained using a 5 mm Doty Scientific magic-angle-spinning probe on a 300 MHz Varian MercuryPlus FT-NMR spectrometer modified with a SpinCore RadioProcessor acquisition system. Samples were spun at 6–12 kHz (as indicated in the figure caption for Fig. 4) and were referenced to $H_3PO_4$, using hydroxyapatite ($Ca_{10}(PO_4)_6(OH)_2$, 2.8 ppm [18]) as a secondary reference. Spectral acquisition used a pulse width of 1.5 μs (~35°), a sweep width of 1 MHz, and 1000–20,000 scans were acquired, depending on the $Rh_2P$ loading. Unsupported $Rh_2P$ was mixed with $Al_2O_3$ prior to analysis in order to fully pack the sample tube.

X-ray photoelectron spectroscopy (XPS) measurements of as-prepared and HDS-tested catalysts were carried out using a Physical Electronics Quantum 2000 Scanning ESCA Microprobe system with a focused monochromatic Al Kα X-ray (1486.7 eV) source and a spherical section analyzer. The XPS measurements were carried out for as-prepared and HDS-tested catalysts following passivation and transfer through air to the spectrometer. The spectra were collected with a pass energy of 23.5 eV. The spectra were referenced to an energy scale with binding energies for $Cu(2p_{3/2})$ at 932.67 ± 0.05 eV and Au(4f) 84.0 ± 0.05 eV. Low energy electrons and argon ions were used for specimen neutralization. Binding energies were corrected for sample charging using the C(1s) peak at 284.6 eV for adventitious carbon as a reference.

BET surface area measurements were acquired using a Micromeritics PulseChemisorb 2700 instrument. Approximately 0.10 g of catalyst was placed in a quartz sample tube and degassed at room temperature in a 60 mL/min He flow for 30 min. The sample was treated in a flow of He (45 mL/min) for 2 h at 623 K and then cooled to room temperature in a continued He flow. The BET measurements were carried out as described elsewhere [19].

Carbon monoxide pulsed chemisorption measurements were also obtained using the Micromeritics PulseChemisorb 2700 instrument. Approximately 0.10 g of catalyst was degassed in 60 mL/min He at room temperature for 30 min. Prior to the measurements, the samples were subjected to one of the following pretreatments: (1) $H_2$ at 573 K; (2) $H_2$ at 573 K, then $H_2S/H_2$ at 573 K; (3) $H_2S/H_2$ at 650 K. For pretreatment #1, samples were heated from room temperature to 573 K in 1 h in a 60 mL/min flow of $H_2$ and held at this temperature for 2 h. For pretreatment #2,

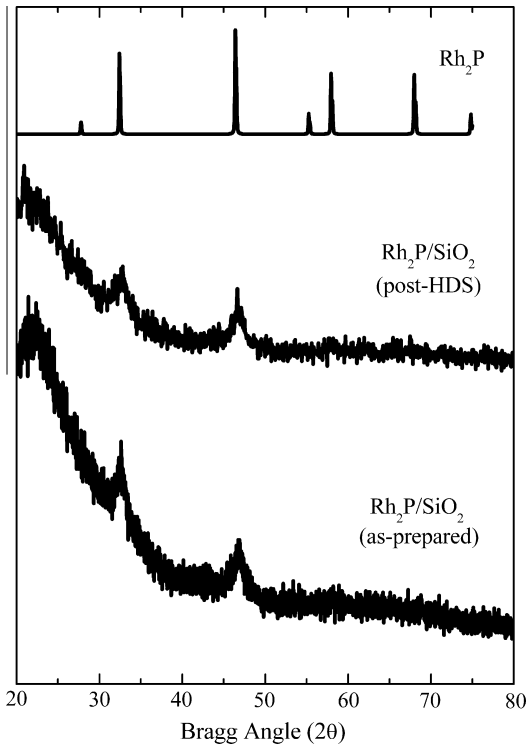


**Fig. 2.** XRD patterns for as-prepared and HDS-tested 5 wt.% $Rh_2P/SiO_2$ catalysts, as well as a reference pattern for $Rh_2P$.

samples were heated from room temperature to 573 K in 1 h in a 60 mL/min flow of $H_2$ and held at this temperature for 2 h, the flow was then switched to 60 mL/min of 3.0 mol% $H_2S/H_2$ mixture for 1 h at 573 K. This pretreatment will be referred to as the "$H_2$ then $H_2S/H_2$" pretreatment. For pretreatment #3, samples were heated from room temperature to 650 K in 1 h in a 60 mL/min flow of a 3.0 mol% $H_2S/H_2$ mixture, held at this temperature for 2 h. Following pretreatments #2 and #3, the samples were subjected to a 60 mL/min flow of $H_2$ at 573 K for 1 h to remove reversibly adsorbed S species. All the samples were then degassed in 45 mL/min He at 573 K for 1 h. Chemisorption capacities were measured by injecting a calibrated sample volume of CO gas (Messer, 99.99%) at 1 min intervals into an He flow (45 sccm/min) passing over the catalyst sample until CO uptake ceased. Prior to injection, the CO was passed through a coil of 1/8″ stainless steel tubing submerged in a pentane slush to remove metal carbonyl impurities. Catalyst samples were maintained at a temperature of 273 K during CO chemisorption measurements. Oxygen ($O_2$) chemisorption capacity measurements for the commercial Ni—Mo/$Al_2O_3$ catalyst following pretreatment with $H_2S/H_2$ were carried out at 196 K using a procedure described elsewhere [19]. A 15.5 mol% $O_2$/He mixture (Airgas) was used for the $O_2$ chemisorption capacity measurements.

Bulk S analyses of catalyst samples were carried out using a LECO SC-144DR Sulfur and Carbon Analyzer after pretreatment as follows. Approximately 0.15 g of catalyst was degassed in 50 mL/min He for 15 min at room temperature. The flow was switched to 60 mL/min $H_2$ and the sample was heated to 573 K in 1 h and held at this temperature for 2 h. The sample was then cooled to room temperature in flowing $H_2$. After cooling, the gas feed was switched to 60 mL/min of 3.0 mol% $H_2S/H_2$. The sample was then heated from room temperature to 573 K in 1 h and held at this temperature for 2 h. The gas feed was then changed to 50 mL/min He and the sample held at 573 K for 1 h. After degassing, the sample was cooled to room temperature and passivated for 2 h in 60 mL/min of 1.0 mol% $O_2$/He. The bulk S (and C) elemental analyses were carried out as follows. Approximately 0.10 g of catalyst was transferred into a ceramic boat. The ceramic boat was then loaded into a furnace where the sample was combusted in an oxygen-rich environment at ~1625 K for 3 min. Combusted carbon ($CO_2$) and sulfur ($SO_2$) that evolved from the catalyst sample was quantified via IR detection and reported as wt.% C and S.

### 2.3. HDS activity measurements

Dibenzothiophene (DBT) HDS activity measurements were carried out using a fixed-bed, continuous flow reactor operating at a total pressure of 3.0 MPa and temperatures in the range 498–573 K. The reactor feed consisted of a decalin solution containing 3000 ppm dibenzothiophene and 500 ppm dodecane, with the latter serving as an internal standard for gas chromatographic analysis of the reactor effluent. The liquid feed (5.4 mL/h) was injected into a 100 mL/min flow of hydrogen and vaporized prior to entry into the reactor. Approximately 0.15 g of catalyst (16–20 mesh size) was diluted with quartz sand to a total volume of 5 mL and loaded into a reactor tube having a diameter of 1.1 cm and length of 40 cm. The reactor temperature was measured with a thermocouple mounted axially in the reactor tube that was in direct contact with the catalyst bed. The 5 wt.% $Rh_2P/SiO_2$ and $Rh/SiO_2$ catalysts were pretreated by heating from room temperature to 573 K in 1 h in a 60 mL/min flow of $H_2$ and held at this temperature for 2 h, then cooled to room temperature in continued $H_2$ flow. Sulfided $Rh/SiO_2$ and commercial Ni—Mo/$Al_2O_3$ catalysts were prepared by heating from room temperature to 650 K in 1 h in a 60 mL/min flow of a 3.0 mol% $H_2S/H_2$ mixture, held at this temperature for 2 h, and then cooled to room temperature in continued gas flow. After pretreatment, with the catalyst samples at room temperature, the reactor was flushed with 60 mL/min He for 30 min and then pressurized to 3.0 MPa with $H_2$. The He (Airgas, 99.999 mol%) and $H_2$ (Airgas, 99.999 mol%) were passed through molecular sieve and $O_2$ removal traps prior to use.

Following pressurization of the reactor with $H_2$, one of three types of HDS activity measurements was carried out. In the first, the catalyst was heated to 498 K in a 150 mL/min flow of $H_2$ over 30 min after which the flow of liquid feed was begun. The reactor was stabilized for approximately 12 h prior to sampling the reactor effluent at 3 h intervals over 12 h. The catalyst temperature was then raised 25 K, the reactor stabilized for 12 h, followed by sampling of the reactor effluent at 3 h intervals. This procedure was repeated until sampling at the maximum catalyst temperature (573 or 598 K) was completed. In the second type of experiment, the catalyst was heated to 573 K in a 150 mL/min flow of $H_2$ over 30 min after which the flow of liquid feed was begun followed by sampling at 1–3 h intervals over a 100 h time period. The third type of experiment investigated the effect of $H_2S$ partial pressure on HDS activity. Dimethyldisulfide (DMDS, Aldrich, 99.0+%) was added to the liquid feed in amounts of 1100 (1 kPa $H_2S$), 3200 (3 kPa $H_2S$), 10,700 (10 kPa $H_2S$), and 53,000 ppm DMDS (50 kPa $H_2S$). Upon changing between feeds with different DMDS

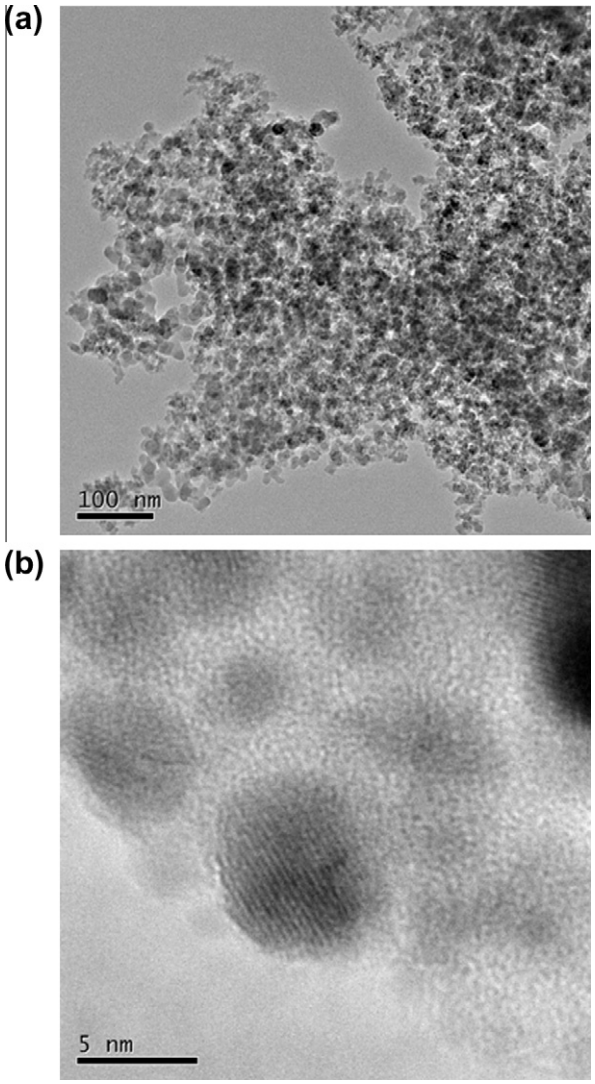


**Fig. 3.** Low- and high-resolution TEM images of a 5 wt.% $Rh_2P/SiO_2$ catalyst.

concentrations, the system was allowed to equilibrate for 3 h and samples were then collected at 1 h intervals. The samples of the liquid reactor effluent from the three types of HDS activity measurements were analyzed off-line using a gas chromatograph (Agilent 6890N) equipped with an HP-5 column and a flame ionization detector.

## 3. Results

### 3.1. Characterization of as-prepared $Rh_2P/SiO_2$ catalysts

The X-ray diffraction pattern for an as-prepared 5 wt.% $Rh_2P/SiO_2$ catalyst is compared to a reference pattern for $Rh_2P$ (card no. 03-065-6417 [20]) in Fig. 2, confirming the phase purity of the silica-supported $Rh_2P$. Using the Scherrer equation, an average $Rh_2P$ crystallite size of 10 nm was calculated for the 5 wt.% $Rh_2P/SiO_2$ catalyst. Low- and high-resolution TEM images of the 5 wt.% $Rh_2P/SiO_2$ catalyst are shown in Fig. 3. The low-resolution image indicates an even dispersion of the $Rh_2P$ particles on the silica support while the high-resolution image shows a globular shaped $Rh_2P$ particle having dimensions of $\sim 7.0 \times 8.5$ nm; The measured spacing between lattice fringes of 0.26 nm is consistent with the d-spacing of 0.275 nm for the (200) crystallographic plane of $Rh_2P$ (card no. 03-065-6417 [20]). Particle size measurements of over thirty $Rh_2P$ particles in a medium-resolution TEM image (not shown) of the 5 wt.% $Rh_2P/SiO_2$ catalyst yielded an average particle size of $3.3 \pm 1.7$ nm, which is significantly smaller than the average crystallite size determined using the Scherrer method. This discrepancy is likely due to the fact that the smallest $Rh_2P$ particles are below the detection limit for XRD, but contribute to the average particle size determined by TEM.

Solid-state $^{31}P$ NMR spectra for unsupported $Rh_2P$ and 5 and 25 wt.% $Rh_2P/SiO_2$ catalysts are shown in Fig. 4. The spectrum for unsupported $Rh_2P$ exhibits a single peak at $\sim$1046 ppm, which indicates that there is a single crystallographic site for P in $Rh_2P$, in agreement with the crystal structure. The large chemical shift results from the Knight shift and is also observed for a number of other metal phosphide phases, including $Ni_2P$ [21], $Ni_3P$ [21,22] and $Cu_3P$ [22] and is indicative of the metallic character of the phase. The $^{31}P$ NMR spectra of the 5 and 25 wt.% $Rh_2P/SiO_2$ catalysts exhibit a similar peak at $\sim$1045 ppm, which is also assigned to P in $Rh_2P$. As the $Rh_2P$ loading decreases, the $^{31}P$ linewidth increases, and linewidth appears to tail off slightly toward higher chemical shift (see Fig. 4). The NMR spectra of the $Rh_2P/SiO_2$ catalysts show additional peaks close to 0 ppm that are assigned to phosphate species at the exterior of the $Rh_2P$ particles or on the silica support. The $^{31}P$ NMR peaks near 0 ppm are similar those observed by Stinner and co-workers for $Ni_2P/SiO_2$ catalysts [21].

Shown in Fig. 5 are XPS spectra in the Rh (3d) and P(2p) regions for an as-prepared 5 wt.% $Rh_2P/SiO_2$ catalyst. The catalyst was passivated in a 1 mol% $O_2$/He mixture following synthesis, which is expected to result in a thin oxidized layer on the exterior of the $Rh_2P$ particles. High-resolution TEM images of a 25 wt.% $Ni_2P/SiO_2$ catalyst showed this layer to be $\sim$2 nm thick on the exterior of the supported $Ni_2P$ particles [23]. While XPS spectra of other metal phosphide catalysts (e.g. $Ni_2P/SiO_2$ [19,23], $Co_xNi_{2-x}P/SiO_2$ [24]) exhibit peaks for both oxidized and reduced metal and P species, only one Rh ($3d_{5/2}$) peak and one P($2p_{3/2}$) peak are apparent for the 5 wt.% $Rh_2P/SiO_2$ catalyst. The XPS spectrum in the Rh $3d_{5/2}$ region shows a peak at 307.8 eV that is slightly above the binding energy for Rh metal (307.0–307.4 eV [25]) and well below the value for $Rh^{3+}$ in $Rh_2O_3$ (308.5 eV [25]), indicating that Rh in $Rh_2P$ bears a partial positive charge ($Rh^{\delta+}$). The peak in the P($2p_{3/2}$) region at 134.3 eV is assigned to $P^{5+}$ species based on its similar binding energy to those for phosphate species [25] and the calcined precursors of other metal phosphide catalysts [19,23,26]. A peak for a reduced P species, observed at 129.5–130.1 eV for $MoP/SiO_2$ [26], $Ni_2P/SiO_2$ [19,23], and $Co_xNi_{2-x}P/SiO_2$ [24] catalysts, is not apparent above the background noise in the P($2p_{3/2}$) region for the 5 wt.% $Rh_2P/SiO_2$ catalyst. This may be due to the substantially lower loading for the $Rh_2P/SiO_2$ catalyst (5 wt.%) than for these other metal phosphide catalysts (20–25 wt.%). The XPS spectrum for an as-prepared 25 wt.% $Rh_2P/SiO_2$ catalyst (not shown) exhibited two peaks in the P($2p_{3/2}$) region having binding energies of 130.0 and 134.0 eV that can be assigned to reduced P species

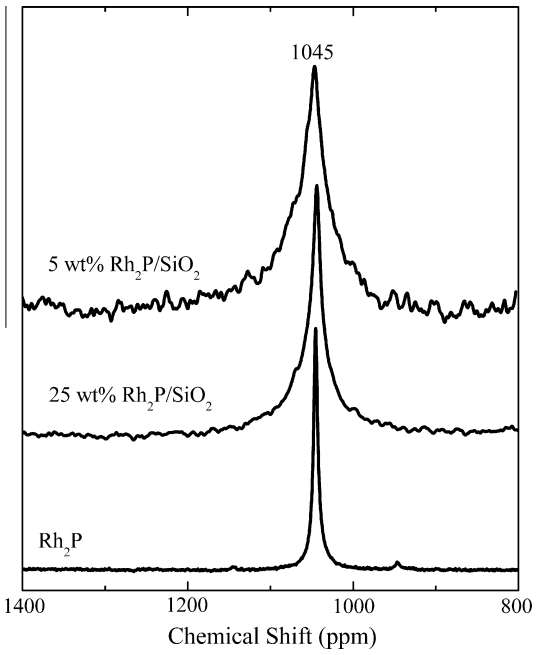


**Fig. 4.** Solid-state $^{31}P$ NMR spectra of unsupported $Rh_2P$ and $Rh_2P/SiO_2$ catalysts. The spinning rates for the $Rh_2P$, 25 wt.% $Rh_2P/SiO_2$, and 5 wt.% $Rh_2P/SiO_2$ samples were 6, 8, and 12 kHz, respectively.

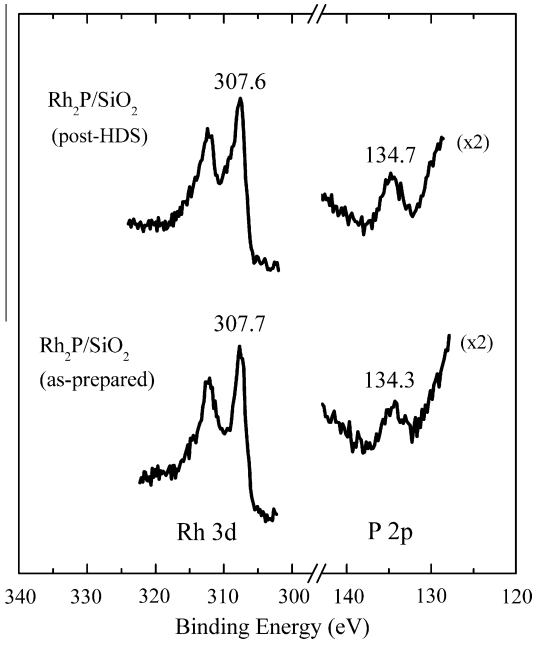


**Fig. 5.** XPS spectra of 5 wt.% $Rh_2P/SiO_2$ and $Rh/SiO_2$ catalysts.

**Table 1**
Catalytic data for Rh phosphide and comparison catalysts.

| Catalyst | BET surface area ($m^2$/g) | Chemisorption capacity (μmol CO/g) | | | DBT HDS activity[a] (nmol DBT/g s) |
|---|---|---|---|---|---|
| | | $H_2$ pretreatment | $H_2 + H_2S/H_2$ pretreatment | $H_2S/H_2$ pretreatment | |
| $Rh_2P/SiO_2$ | 128 | 68 | 41 | – | 145 |
| $Rh/SiO_2$ | 142 | 72 | 22 | – | 44 |
| Sulf. $Rh/SiO_2$ | 139 | – | – | 18 | 102 |
| Sulf. Ni—$Mo/Al_2O_3$ | 110 | – | – | 65[b] | 123 |

[a] HDS activity at 548 K.
[b] Oxygen chemisorption (μmol $O_2$/g) at 196 K.

(bonded to P in $Rh_2P$) and $P^{5+}$ species in the passivation layer around the phosphide particles. A surface composition of $Rh_{1.94}P_{1.00}$ was determined from the XPS data for the as-prepared 5 wt.% $Rh_2P/SiO_2$ catalyst, which is close to the expected bulk composition of $Rh_2P$.

The BET surface areas and chemisorption capacities for the 5 wt.% $Rh_2P/SiO_2$ and comparison catalysts are listed in Table 1. The $Rh_2P/SiO_2$ and $Rh/SiO_2$ catalysts had similar CO chemisorption capacities following pretreatment with $H_2$. The chemisorption capacities of catalysts were substantially lower following sequential pretreatment with $H_2$ and then $H_2S/H_2$, but the $Rh_2P/SiO_2$ catalyst adsorbed nearly twice as much CO than did the $Rh/SiO_2$ catalyst in this case. The sulfided $Rh/SiO_2$ catalyst adsorbed the least CO of the Rh catalysts. Low temperature oxygen chemisorption, which is typically used to estimate site densities for sulfided Ni—Mo catalysts, yielded a chemisorption capacity of 65 μmol/g for the commercial Ni—$Mo/Al_2O_3$ catalyst. This is similar to the CO chemisorption capacities measured for the $Rh_2P/SiO_2$ and $Rh/SiO_2$ catalysts pretreated with $H_2$.

### 3.2. Dibenzothiophene HDS activity and selectivity of $Rh_2P/SiO_2$ catalysts

Dibenzothiophene HDS activity measurements were carried out for 5 wt.% $Rh_2P/SiO_2$ catalysts as a function of reaction temperature, time on stream, and in the presence of different partial pressures of $H_2S$. For comparison purposes, DBT HDS measurements were also conducted for $Rh/SiO_2$ and sulfided $Rh/SiO_2$ catalysts, as well as for a commercial Ni—$Mo/Al_2O_3$ catalyst. Shown in Fig. 6 are the DBT conversions for the different catalysts over the temperature range 498–598 K. The 5 wt.% $Rh_2P/SiO_2$ catalyst exhibited the highest DBT conversion of the catalysts investigated at all temperatures, with essentially 100% DBT conversion observed at 548 K and above. At 548 K, the DBT conversions increase in the order $Rh/SiO_2$ < sulfided $Rh/SiO_2$ < sulfided Ni—$Mo/Al_2O_3$ < $Rh_2P/SiO_2$. The HDS activity of the 5 wt.% $Rh_2P/SiO_2$ catalyst at 548 K was 145 nmol DBT/$g_{cat}$·s, which compares favorably with that of 123 nmol DBT/$g_{cat}$·s for the commercial Ni—$Mo/Al_2O_3$ catalyst. We previously reported that a 25 wt.% $Ni_2P/SiO_2$ catalyst had a DBT HDS activity of 106 nmol DBT/$g_{cat}$·s under the same reaction conditions [15]; despite the $Rh_2P/SiO_2$ catalyst having a loading one-fifth that of the $Ni_2P/SiO_2$ catalyst, the Rh phosphide catalyst is 37% more active than the Ni phosphide catalyst. The $Rh/SiO_2$ and sulfided $Rh/SiO_2$ catalysts, having DBT HDS activities of 44 and 102 nmol DBT/$g_{cat}$·s at 548 K, are less active than the 5 wt.% $Rh_2P/SiO_2$ and commercial Ni—$Mo/Al_2O_3$ catalysts. Consistent with our results, Brenner et al. [27] observed a sulfided 10 wt.% $Rh/Al_2O_3$ catalyst to be less active (at 623 K) than a commercial Ni—$Mo/Al_2O_3$ catalyst for DBT HDS. There are conflicting results in the literature regarding the effect of pretreatment on HDS activity for supported Rh catalysts, with $H_2$ pretreatment yielding the highest activity for a 1 wt.% $Rh/SiO_2$ catalyst [28] and $H_2S/H_2$ [29] or $H_2S$ [12] for 2 wt.% $Rh/Al_2O_3$ catalysts. The reasons for the different DBT HDS results for $Rh/SiO_2$ and sulfided $Rh/SiO_2$ catalysts are

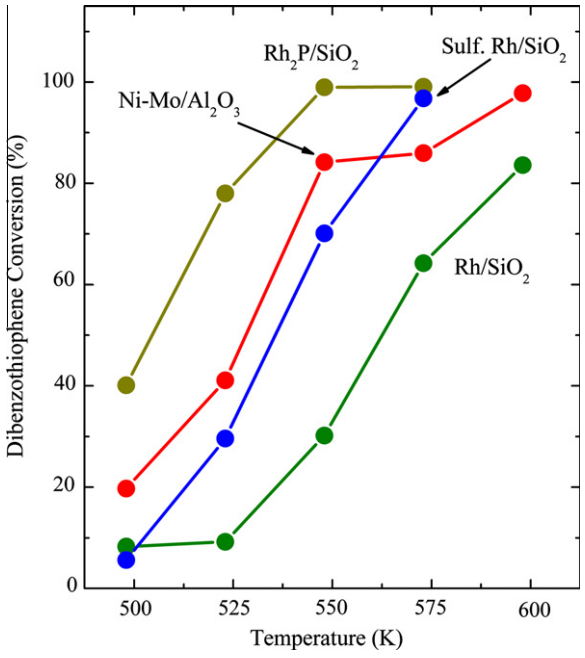


**Fig. 6.** DBT conversions vs. reaction temperature.

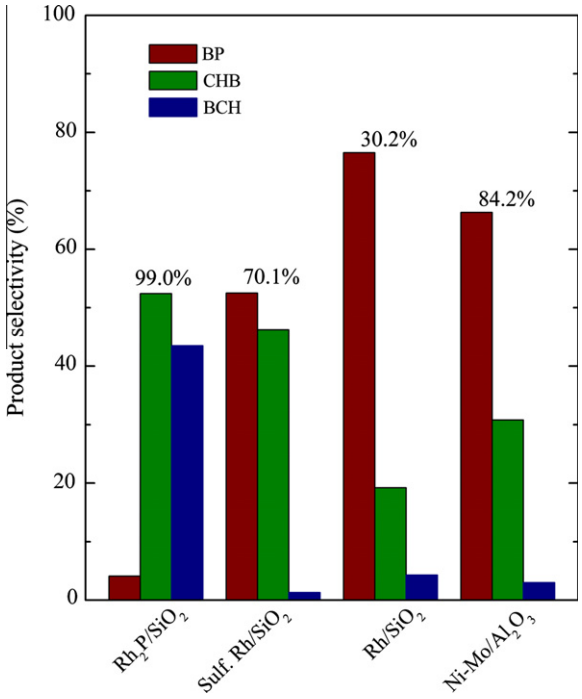


**Fig. 7.** DBT HDS product distributions at 548 K. The DBT HDS conversions at 548 K are listed above the product distributions for each catalyst.

unclear, but the Rh precursor, Rh loading, oxide support, pretreatment and HDS conditions are likely important factors.

The DBT HDS product selectivities at 548 K are shown in Fig. 7 for the 5 wt.% $Rh_2P/SiO_2$ and the comparison catalysts. The commercial Ni—Mo/$Al_2O_3$ catalyst favored the direct desulfurization (DDS) pathway with a biphenyl (BP) selectivity of 66%. The remainder of the DBT converted reacted via the hydrogenation (HYD) pathway, yielding cyclohexylbenzene (CHB) and bicyclohexane (BCH) with selectivities of 31% and 3%, respectively. This selectivity is similar to that reported by others for DBT HDS over sulfided Ni—Mo/$Al_2O_3$ catalysts at 523–613 K [27,30]. The 5 wt.% $Rh_2P/SiO_2$ catalyst strongly favored the HYD pathway (96%) at 548 K, with CHB and BCH selectivities of 52% and 44%, respectively. This product selectivity was dramatically different from that of the less active $Rh/SiO_2$ and sulfided $Rh/SiO_2$ catalysts, which favored the DDS pathway and produced very little BCH (see Fig. 7).

To assess the stability of the 5 wt.% $Rh_2P/SiO_2$ catalyst in HDS processing conditions, two experiments were performed. In the first, a sample of the 5 wt.% $Rh_2P/SiO_2$ catalyst was subjected to a 100 h DBT HDS measurement at 573 K; the DBT conversion and product selectivity are plotted in Fig. 8. The DBT conversion over the 5 wt.% $Rh_2P/SiO_2$ catalyst held steady at 94–99% during the 100 h measurement with no indication of deactivation over time. Interestingly, the product distribution changed over time. While the selectivity toward CHB was steady at 54–59% over the 100 h period, the BP selectivity increased steadily from 6% to almost 20% and the BCH selectivity decreased from 40% to 23%. In the second experiment, the DBT HDS conversions of 5 wt.% $Rh_2P/SiO_2$ and $Rh/SiO_2$ catalysts were measured while co-feeding increasing amounts of $H_2S$ (0–50 kPa) with the 3000 ppm DBT reactor feed. The DBT conversions for the two catalysts are plotted vs. $H_2S$ partial pressure (0–10 kPa) in Fig. 9. Following an initial stabilization of the catalysts for 3 h on stream with no $H_2S$ co-feeding, the 5 wt.% $Rh_2P/SiO_2$ and $Rh/SiO_2$ catalysts had DBT conversions of 79% and 65%, respectively. Upon co-feeding 1 kPa $H_2S$, the DBT conversions of the $Rh_2P/SiO_2$ and $Rh/SiO_2$ catalysts decreased significantly to 38% and 20%, respectively. These decreases correspond to a twofold decrease in DBT conversion for the $Rh_2P/SiO_2$ catalyst

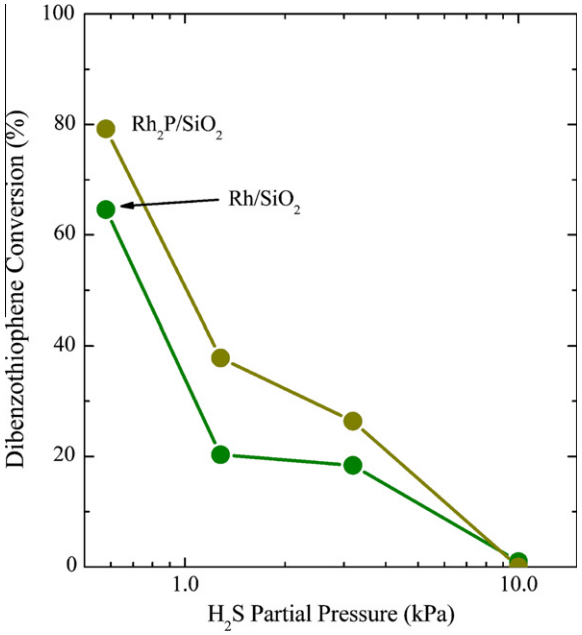


**Fig. 9.** Effect of $H_2S$ partial pressure on DBT conversion at 573 K.

and threefold decrease for the $Rh/SiO_2$ catalyst, indicating a stronger sensitivity to $H_2S$ for the Rh metal catalyst. The DBT conversions for the two catalysts decreased further upon increasing the partial pressure of co-fed $H_2S$ to 3, 10, and 50 kPa, with no conversion measured for an $H_2S$ partial pressure of 10 kPa or higher. After completion of the 50 kPa $H_2S$ co-feeding, the DBT reactor feed was continued for 3 h and the conversions were measured. Partial recovery of HDS activity was observed for both catalysts, with the $Rh_2P/SiO_2$ catalyst having a DBT conversion 24% and the $Rh/SiO_2$ catalyst having a conversion of 13% (see Fig. 10). Compared to their DBT conversions prior to $H_2S$ co-feeding, the $Rh_2P/SiO_2$

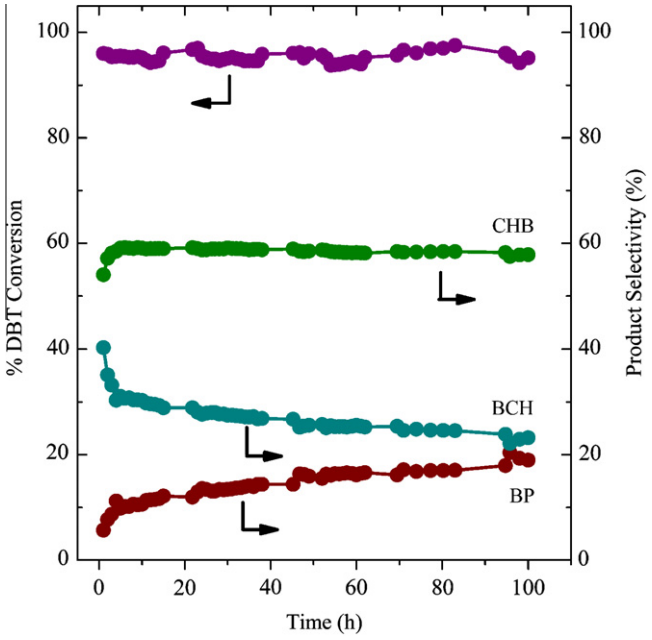


**Fig. 8.** DBT conversion and product selectivity at 573 K vs. time for a 5 wt.% $Rh_2P/SiO_2$ catalyst.

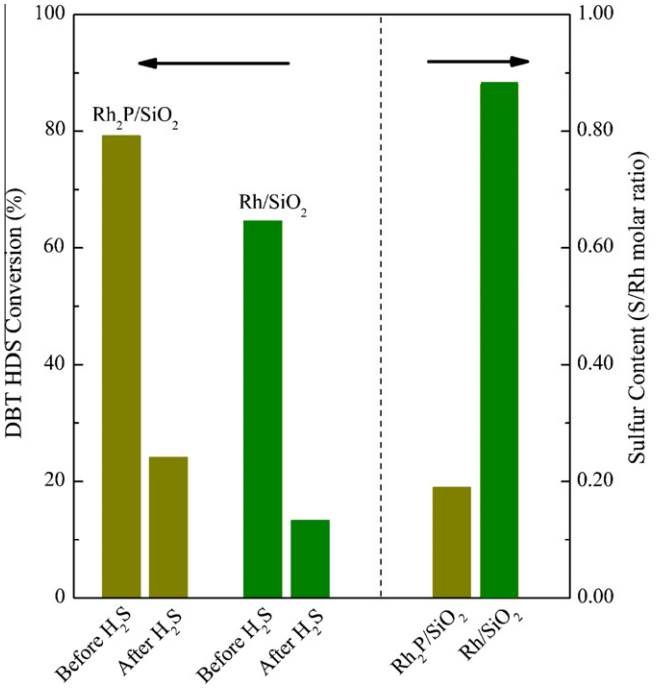


**Fig. 10.** DBT HDS conversion before and after co-feeding 50 kPa $H_2S$, and catalyst S content after treatment with $H_2S/H_2$.

catalyst recovered 30% of its initial HDS activity while the $Rh/SiO_2$ catalyst recovered just 20% of its initial activity, indicating a stronger S poisoning of the $Rh/SiO_2$ catalyst.

### 3.3. Characterization of HDS-tested and $H_2S/H_2$-treated $Rh_2P/SiO_2$ catalysts

The 5 wt.% $Rh_2P/SiO_2$ catalyst exhibited excellent stability during HDS testing and better resistance to S poisoning than did the $Rh/SiO_2$ catalyst. An XRD pattern of a 5 wt.% $Rh_2P/SiO_2$ catalyst after DBT HDS activity measurement is shown in Fig. 2; there is no evidence for the formation of new Rh-containing phases, and there was no appreciable change in the $Rh_2P$ crystallite size for the HDS-tested catalyst. The XPS spectrum of an HDS-tested $Rh_2P/SiO_2$ catalyst is shown in Fig. 3, and no significant changes are apparent. No sulfur signal was apparent above the background noise in the S(2p) region; a surface composition of $Rh_{1.76}P_{1.00}S_{\leqslant 0.06}$ was determined for the HDS-tested catalyst. Relative to the surface composition of the as-prepared 5 wt.% $Rh_2P/SiO_2$ catalyst ($P^s/Rh^s = 0.52$), a small P enrichment of the surface was observed for the HDS-tested catalyst ($P^s/Rh^s = 0.57$), where the "s" superscripts refer to the surface molar ratios determined by XPS.

To further probe the effect of S on the 5 wt.% $Rh_2P/SiO_2$ and $Rh/SiO_2$ catalysts, the CO chemisorption capacities and S contents were measured for samples treated with $H_2S/H_2$ following the pretreatment with $H_2$ that was used prior to DBT HDS testing. As listed in Table 1, the CO chemisorption capacities of the catalysts treated with $H_2$ and then $H_2S/H_2$ are significantly less than the catalysts pretreated with $H_2$ only. The CO chemisorption capacity of the $Rh_2P/SiO_2$ catalyst decreased from 68 to 41 μmol/g (~40% decrease), while the decrease from 72 to 22 μmol/g (~70%) for the $Rh/SiO_2$ catalyst was substantially larger. The S contents measured for 5 wt.% $Rh_2P/SiO_2$ and $Rh/SiO_2$ catalysts treated with $H_2$ and then $H_2S/H_2$ (see Fig. 10) show that the $Rh_2P/SiO_2$ incorporated significantly less S (S/Rh = 0.19) than did the $Rh/SiO_2$ catalyst (S/Rh = 0.88).

## 4. Discussion

A number of monometallic phosphide (e.g. MoP, WP, CoP, $Co_2P$, $Ni_2P$) and bimetallic phosphide (e.g. NiMoP, $Ni_xMoP$, $Co_xNi_2P$, $Co_xNi_{2-x}P$, $Fe_xNi_{2-x}P$) phases have been the focus of research efforts aimed at developing alternatives to metal sulfide catalysts for use in hydrotreating applications [14]. Among monometallic phosphides, $Ni_2P$ has exhibited the highest HDS activities [19,21,23,31–49], while Ni-rich bimetallic phosphides have shown the high activities among this class of phosphides [15,44,50,51]. To the best of our knowledge, the HDS properties of noble metal phosphides have not been reported in the literature despite the fact that noble metals [7–13] and noble metal sulfides [1–6] exhibit high HDS activities. As discussed below, silica-supported $Rh_2P$ exhibits strong HDS properties, with DBT HDS activities higher than that of $Rh/SiO_2$ and sulfided $Rh/SiO_2$ catalysts.

### 4.1. Solid-state and surface chemistry of $Rh_2P$

As shown in Fig. 1, $Rh_2P$ adopts the anti-fluorite structure ($Fm\bar{3}m$ space group) in which the Rh atoms occupy tetrahedral positions and the P atoms occupy cubic positions in the lattice [17]. The lattice constant for $Rh_2P$ was determined to be 0.5498 nm with Rh—Rh and Rh—P distances of 0.2749 and 0.2381 nm, respectively [17,52]. By comparison, an Rh-Rh distance of 0.269 nm for bulk Rh metal can be calculated from its lattice parameter value of 0.380 nm [53]. Consistent with these Rh—Rh distances for $Rh_2P$ and Rh metal, electronic structure calculations for $Rh_2P$ indicate that the bonding is dominated by Rh—P interactions, with Rh—Rh and P—P interactions being substantially weaker [54].

As confirmed by XRD, silica-supported $Rh_2P$ was prepared by TPR of a Rh phosphate-like precursor, with the precursor prepared by impregnation of silica with an aqueous solution of rhodium chloride and ammonium dihydrogen phosphate followed by calcination. To the best of our knowledge, this is the first report of the preparation of a supported noble metal phosphide catalyst by TPR of a phosphate-like precursor in hydrogen. Muetterties et al. [55] described the synthesis of phosphided Pd, Pt, Rh, and Ru on alumina prepared by treating the supported metals with a 25 mol% phosphine ($PH_3$)/He mixture at 523–573 K for 3 h. No XRD peaks were observed for the phosphided $Rh/Al_2O_3$ or $Ru/Al_2O_3$ catalysts, but peaks associated with crystalline $PtP_2$ for the phosphided $Pt/Al_2O_3$ catalyst, and $Pd_6P$ and $Pd_5P_2$ for the phosphided $Pd/Al_2O_3$ catalyst were observed. In the current study, the average $Rh_2P$ crystallite size of 10 nm determined using the Scherrer equation for the TPR-prepared 5 wt.% $Rh_2P/SiO_2$ catalyst, and the smaller average particle size of 3.3 nm determined by TEM indicate that highly dispersed $Rh_2P$ particles were prepared on the $SiO_2$ support despite the high temperature (923 K) used in the TPR synthesis. Solid-state $^{31}P$ NMR spectroscopy of the unsupported $Rh_2P$ and $Rh_2P/SiO_2$ catalysts indicates that the Rh phosphide is metallic, which is consistent with observations for some other metal-rich phosphide phases ($Ni_2P$ [21], $Ni_3P$ [21,22], $Cu_3P$ [22]). It was reported previously that bulk $Rh_2P$ is metallic and exhibits superconducting properties below ~1.3 K [54]. The $^{31}P$ NMR linewidth for the peak at ~1045 ppm increases as the $Rh_2P$ loading decreases from unsupported $Rh_2P$ to 25 and 5 wt.% $Rh_2P$ in the supported catalysts. This most likely reflects the presence of a broader range of chemical environments for P as the $Rh_2P$ loading (and particle size) decreases, due to the increase in the surface-to-volume ratio for the supported $Rh_2P$ particles.

The surface composition measured for the as-prepared 5 wt.% $Rh_2P/SiO_2$ catalyst, $Rh_{1.94}P_{1.00}$, is close to the expected bulk composition of $Rh_2P$. The Rh $3d_{5/2}$ binding energy of 307.8 eV indicates that Rh in the $Rh_2P/SiO_2$ catalyst bears a partial positive charge ($Rh^{\delta+}$), but determination of the oxidation state of the Rh is complicated by the presence of a passivation layer on the surface of the as-prepared $Rh_2P$ particles. The fact that the Rh $3d_{5/2}$ binding energy is just above that for Rh metal ((307.0–307.4 eV [25]) could be due to oxidized Rh species in the passivation layer. As discussed above, the $^{31}P$ NMR spectral data indicate that the silica-supported $Rh_2P$ particles are metallic, suggesting that the Rh oxidation state is close to zero. The 5 wt.% $Rh_2P/SiO_2$ catalyst had a CO chemisorption capacity of 68 μmol/g, which is slightly less than the value of 72 μmol/g measured for the $Rh/SiO_2$ catalyst having a similar Rh loading. While the $Rh_2P/SiO_2$ and $Rh/SiO_2$ catalysts treated with $H_2$ had similar CO chemisorption capacities, pretreatment of the catalysts with $H_2$ then $H_2S/H_2$ resulted in dramatically higher site blockage for the $Rh/SiO_2$ catalyst (22 μmol/g) than for the $Rh_2P/SiO_2$ catalyst (41 μmol/g) as measured by CO chemisorption. The results of S content analyses of the catalysts subjected to the $H_2$ then $H_2S/H_2$ pretreatment indicate that the site blockage is due to strongly bonded S species, with the $Rh/SiO_2$ catalyst (S/Rh = 0.88) having an S content over 4.5 times higher than that of the $Rh_2P/SiO_2$ catalyst (S/Rh = 0.19). Chuang et al. [56] used IR spectroscopy to probe the adsorption of CO on a 3 wt.% $Rh/SiO_2$ catalyst pretreated with either $H_2$ at 673 K, or $H_2$ (673 K) then 1000 ppm $H_2S/H_2$ (513–673 K), followed by $H_2$ at 673 K. The latter treatment is similar to the "$H_2$ then $H_2S/H_2$" pretreatment used in the current study except that the $H_2S$ concentration and pretreatment temperatures were different. For the $H_2$-treated catalyst, two CO absorbances were observed at 2044 and 1890 $cm^{-1}$ that were assigned to linear and bridge bonded CO species, respectively.

Following pretreatment with $H_2$ then $H_2S/H_2$, which yielded a $Rh/SiO_2$ catalyst having S/Rh = 0.12, the linear bonded CO absorbance increased slightly in intensity and shifted to 2062 $cm^{-1}$, while the bridge bonded CO absorbance decreased dramatically and shifted to ~1870 $cm^{-1}$. The authors concluded that the strongly adsorbed S species on the surface isolated the remaining Rh sites on the catalyst, disrupting the formation of bridge bonded CO species, and also weakened the adsorption of linear CO species by withdrawing electron density from Rh sites. The hydrogen chemisorption capacity of the $H_2$-treated 3 wt.% $Rh/SiO_2$ catalyst was 9.8 μmol/g and that of the $H_2$ then $H_2S/H_2$-treated catalyst was below 0.5 μmol/g [56], indicating that H adsorption was strongly suppressed by the surface S. Carbon monoxide hydrogenation activity measurements over the $Rh/SiO_2$ catalyst revealed that the $H_2$ then $H_2S/H_2$ treatment resulted in strongly decreased hydrogenation activity (relative to the $H_2$ treatment), which was attributed to the suppression of dissociative hydrogen adsorption and weakening of CO adsorption due to the irreversibly adsorbed S. Ethylene hydrogenation over the $Rh/SiO_2$ catalyst was also strongly suppressed by the irreversibly adsorbed S species on the Rh metal particles. As discussed below, these results are consistent with the HDS catalytic properties observed for the $Rh/SiO_2$, sulfided $Rh/SiO_2$, and $Rh_2P/SiO_2$ catalysts in the current study.

Some evidence for the catalytic properties of phosphided $Rh/Al_2O_3$ is available from a study by Muetterties et al. [55]. The hydrogenation properties of $Rh/Al_2O_3$ treated with $H_2$, $Rh/Al_2O_3$ treated with 25 mol% $PH_3$/He at 523–573 K, and $Rh/Al_2O_3$ treated with $H_2S$/He at 348–423 K were investigated. The phosphided $Rh/Al_2O_3$ catalyst had Rh and P contents of 5%; although not stated, it is assumed that these percentages are on a weight basis. These percentages indicate a very P-rich phase (P/Rh = 3.3), but the authors believe as much as 1–1.5% of the P was associated with the $Al_2O_3$ support. For the hydrogenation of 1-butene, $Rh/Al_2O_3$ had a substantially higher activity than did the phosphided and sulfided $Rh/Al_2O_3$ catalysts at 348 K. Comparing the phosphided and sulfided $Rh/Al_2O_3$ catalysts, the Rh sulfide catalyst was more active for isomerization of 1-butene to cis- and trans-2-butene than was the phosphided $Rh/Al_2O_3$ catalyst at 348 K. These results are not consistent with those observed in the current study, which we attribute to the P-rich nature of the phosphided $Rh/Al_2O_3$ catalyst investigated by Muetterties et al. [55].

### 4.2. HDS properties of $Rh_2P/SiO_2$ catalysts

The 5 wt.% $Rh_2P/SiO_2$ catalyst investigated in this study exhibited very high DBT HDS activity as well as excellent stability under HDS processing conditions. The $Rh_2P/SiO_2$ catalyst had a higher DBT conversion than $Rh/SiO_2$ and sulfided $Rh/SiO_2$ catalysts having the same Rh loading and was also more active than a commercial Ni—$Mo/Al_2O_3$ catalyst over the temperature range 498–573 K. At a temperature of 573 K, the DBT conversion for a 5 wt.% $Rh_2P/SiO_2$ catalyst was essentially constant (94–99%) over a 100 h test period. XRD and XPS analyses of HDS-tested 5 wt.% $Rh_2P/SiO_2$ catalysts indicated no significant changes in the phase purity, crystallite size and chemical composition of the Rh phosphide catalysts as a result of HDS processing. On a mass of catalyst basis, the 5 wt.% $Rh_2P/SiO_2$ catalyst is somewhat more active for DBT HDS at 548 K than 25 wt.% $Ni_2P/SiO_2$ and $Fe_{0.03}Ni_{1.97}P/SiO_2$ catalysts tested under similar conditions in our laboratory [15], and the Rh phosphide is dramatically more active on a mol metal basis. The 5 wt.% $Rh_2P/SiO_2$ catalyst is 37% and 22% more active than the 25 wt.% $Ni_2P/SiO_2$ and $Fe_{0.03}Ni_{1.97}P/SiO_2$ catalysts, respectively, on a mass of catalyst basis. As shown in Fig. 11, the 5 wt.% $Rh_2P/SiO_2$ catalyst is almost eleven times more active than the 25 wt.% $Ni_2P/SiO_2$ catalyst on a mol metal basis, and ten times more active than the 25 wt.% $Fe_{0.03}Ni_{1.97}P/SiO_2$ catalyst. The 5 wt.% $Rh_2P/SiO_2$ catalyst is also significantly more active than the $Rh/SiO_2$ and sulfided $Rh/SiO_2$ catalysts; all the Rh catalysts are more active than the 25 wt.% $Ni_2P/SiO_2$ and $Fe_{0.03}Ni_{1.97}P/SiO_2$ catalysts. Finally, the Rh catalysts can be compared using their CO chemisorption capacities to calculate turnover frequencies (TOFs). In doing so, we make the assumption that the chemisorption capacities measured after the $H_2$ then $H_2S/H_2$ pretreatment provide the best estimate of the active site densities on the $Rh_2P/SiO_2$ and $Rh/SiO_2$ catalysts. TOFs of $3.6 \times 10^{-4}$, $2.0 \times 10^{-4}$, and $5.7 \times 10^{-4}$ can be calculated for the 5 wt.% $Rh_2P/SiO_2$, $Rh/SiO_2$, and sulfided $Rh/SiO_2$ catalysts, respectively. The sulfided $Rh/SiO_2$ catalyst has the highest TOF; the higher overall DBT HDS activity of the $Rh_2P/SiO_2$ is a result of its combination of high TOF and site density.

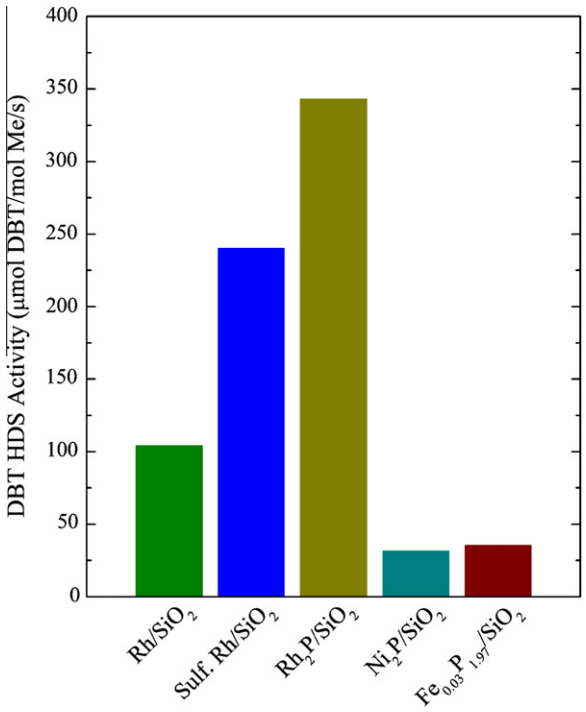


**Fig. 11.** DBT HDS activities normalized per mol of metal.

The DBT HDS product selectivity for the 5 wt.% $Rh_2P/SiO_2$ catalyst is substantially different from those of the $Rh/SiO_2$ and sulfided $Rh/SiO_2$ catalysts, as well as that for the commercial Ni—$Mo/Al_2O_3$ catalyst. At 548 K, the 5 wt.% $Rh_2P/SiO_2$ catalyst strongly favors the HYD pathway (96%) in which one or both benzene rings are hydrogenated prior to cleavage of the C—S bonds. This is markedly different from the $Rh/SiO_2$ and commercial Ni—$Mo/Al_2O_3$ catalysts, which favor the DDS pathway (76% and 66%, respectively). The sulfided $Rh/SiO_2$ catalyst is almost evenly split between the DDS (52%) and HYD (48%) pathways for DBT HDS.

We attribute the excellent hydrogenation properties of the 5 wt.% $Rh_2P/SiO_2$ catalyst to the metallic nature of the $Rh_2P$ and its strong resistance to S incorporation. While noble metals are well-known hydrogenation catalysts, they are highly sensitive to S poisoning. This is the likely reason why the $Rh/SiO_2$ catalyst has a substantially lower DBT HDS activity than the $Rh_2P/SiO_2$ catalyst in the relatively S-rich feed (3000 ppm DBT) used in the activity measurements. When subjected to the $H_2$ then $H_2S/H_2$ pretreatment, the $Rh/SiO_2$ catalyst accumulated over four times more S than did the $Rh_2P/SiO_2$ catalyst and the product selectivities suggest that the blocked sites on $Rh/SiO_2$ catalyst are ones on which HDS takes place via the HYD pathway. The 100 h DBT HDS measurement for the 5 wt.% $Rh_2P/SiO_2$ catalyst suggests that some HYD sites on the phosphide catalyst are susceptible to poisoning by

S also, but not at the expense of overall HDS activity. After bringing the $Rh_2P/SiO_2$ catalyst on stream, the selectivity toward BP was 5–10%, while the selectivity toward the HYD products was 90–95%. Over the course of the 100 h reaction, the DBT conversion was steady at 94–99%, but the selectivity toward BP gradually increased to ~20% while the selectivity toward BCH decreased from ~40% to 22%. During the 100 h measurement, the CHB selectivity remained steady at 55–58%, which is surprising given the changes in BP and BCH selectivities. The selectivity results suggest a direct relationship between BP and BCH but we could not find evidence in the literature for a reaction network incorporating a direct link between these products.

### 4.3. Sulfur tolerance of $Rh_2P/SiO_2$ catalysts

The 5 wt.% $Rh_2P/SiO_2$ catalyst showed excellent resistance to deactivation by sulfur, which is consistent with previous reports for other metal phosphide catalysts. In particular, highly active $Ni_2P/SiO_2$ [23,38,57] and Ni-rich bimetallic phosphide ($Co_xNi_{2-x}P/SiO_2$ [24], $Fe_xNi_{2-x}P/SiO_2$ [15]) catalysts incorporated remarkably low amounts of S during HDS processing or treatment with $H_2S/H_2$. XPS analysis of an HDS-tested 5 wt.% $Rh_2P/SiO_2$ catalyst showed no evidence for surface sulfur in the S(2p) region and bulk S analysis of a $H_2$, then $H_2S/H_2$-treated $Rh_2P/SiO_2$ catalyst yielded a S content corresponding to S/Rh = 0.19. By comparison, a $Rh/SiO_2$ catalyst treated similarly had a S content of S/Rh = 0.88, which is over four times greater than for the phosphide catalyst. The resistance to S incorporation of the $Rh_2P/SiO_2$ catalyst is attributed to the P in the $Rh_2P$ particles, which inhibits the irreversible adsorption of S at the particle surface as well as the incorporation of S into the bulk (i.e. to form Rh sulfide). As described earlier, bonding in $Rh_2P$ is dominated by Rh—P interactions [54], as indicated by an Rh—P distance (0.2381 nm) that is shorter than the Rh—Rh distance (0.2749 nm) [17,52]. There was no evidence for loss of phase purity or crystallite growth for the $Rh_2P$ particles during HDS processing; in addition to no detectable surface sulfur, XPS analysis of an HDS-tested catalyst showed a slight enrichment of P at the surface ($P^s/Rh^s = 0.57$ relative to the as-prepared $Rh_2P/SiO_2$ catalyst ($P^s/Rh^s = 0.52$). While we conclude that surface P inhibits the incorporation of irreversibly bonded S on the $Rh_2P$ particles, the surface P does not appear to suppress CO adsorption. Hydrogen-pretreated $Rh/SiO_2$ and $Rh_2P/SiO_2$ catalysts had similar CO chemisorption capacities (72 and 68 μmol/g, respectively). An IR spectroscopy investigation of CO adsorption on $Ni/SiO_2$ and $Ni_2P/SiO_2$ catalysts revealed that surface P hindered the formation of bridge bonded CO, but that surface P also adsorbed CO via the formation of P═C═O species [39]. Adsorption of linearly bonded CO was enhanced on the $Ni_2P/SiO_2$ catalyst (relative to $Ni/SiO_2$), and the Ni phosphide catalyst adsorbed more CO overall than did the $Ni/SiO_2$ catalyst when pretreated with either $H_2$ or $H_2S/H_2$. The $Rh/SiO_2$ and $Rh_2P/SiO_2$ catalysts had markedly different chemisorption capacities after pretreatment with $H_2$ then $H_2S/H_2$, with the $Rh/SiO_2$ catalyst (22 μmol/g) adsorbing just over one-half the amount of the $Rh_2P/SiO_2$ catalyst (41 μmol/g). This result further indicates that P in $Rh_2P$ increases the sulfur tolerance of Rh by inhibiting the formation of irreversibly adsorbed S species while not blocking CO adsorption. Most importantly, the higher DBT HDS activity of the 5 wt.% $Rh_2P/SiO_2$ catalyst indicates that the presence of P in this catalyst enhances the HDS catalytic properties of Rh.

## 5. Conclusions

$Rh_2P/SiO_2$ catalysts having well-dispersed $Rh_2P$ particles were prepared by temperature-programmed reduction of oxidic precursors in flowing $H_2$. The silica-supported $Rh_2P$ particles are metallic in nature and have a surface composition of $Rh_{1.94}P_{1.00}$ that is similar to that expected from the bulk stoichiometry. A 5 wt.% $Rh_2P/SiO_2$ catalyst exhibited excellent DBT HDS properties, having a higher activity than $Rh/SiO_2$ and sulfided $Rh/SiO_2$ catalysts and a commercial Ni—$Mo/Al_2O_3$ catalyst. The $Rh_2P/SiO_2$ catalyst showed excellent stability over a 100 h DBT HDS activity measurement, was more S tolerant than the $Rh/SiO_2$ catalyst, and strongly favored the HYD pathway for DBT HDS. These results suggest that $Rh_2P/SiO_2$ catalysts have strong potential for deep HDS processing.

## Acknowledgments

This research was supported by the National Science Foundation under grant number CHE-0809433. A portion (XPS, TEM) of the research described in this paper was performed in the Environmental Molecular Sciences Laboratory (EMSL), a national scientific user facility sponsored by the Department of Energy's Office of Biological and Environmental Research and located at Pacific Northwest National Laboratory. The authors would like to acknowledge ConocoPhillips (Ferndale refinery) for providing access to the LECO SC-144DR Sulfur and Carbon Analyzer.

## References

[1] T.A. Pecoraro, R.R. Chianelli, J. Catal. 67 (1981) 430.
[2] J.P.R. Vissers, C.K. Groot, E.M. van Oers, V.H.J. de Beer, R. Prins, Bull. Soc. Chim. Belg. 93 (1984) 813.
[3] M.J. Ledoux, O. Michaux, G. Agostini, J. Catal. 102 (1986) 275.
[4] J. Frimmel, M. Zdrazil, J. Catal. 167 (1997) 286.
[5] A.P. Raje, S.J. Liaw, B.H. Davis, Appl. Catal. 150 (1997) 297.
[6] E.J.M. Hensen, H.J.A. Brans, G.M.H.J. Lardinois, V.H.J. de Beer, J.A.R. van Veen, R.A. van Santen, J. Catal. 192 (2000) 98.
[7] H.R. Reinhoudt, R. Troost, A.D. van Langeveld, S.T. Sie, J.A.R. van Veen, J.A. Moulijn, Fuel Process. Technol. 61 (1999) 133.
[8] V.L. Barrio, P.L. Arias, J.F. Cambra, M.B. Güemez, B. Pawelec, J.L.G. Fierro, Fuel 82 (2003) 501.
[9] A. Ishihara, F. Dumeignil, J. Lee, K. Mitsuhashi, E.W. Qian, T. Kabe, Appl. Catal. A 289 (2005) 163.
[10] A. Niquille-Röthlisberger, R. Prins, J. Catal. 242 (2006) 207.
[11] A. Niquille-Röthlisberger, R. Prins, Catal. Today 123 (2007) 198.
[12] S.A. Giraldo, M.H. Pinzon, A. Centeno, Catal. Today 133–135 (2008) 239.
[13] Y. Kanda, A. Seino, T. Kobayashi, Y. Uemichi, M. Sugioka, J. Jpn. Petrol. Inst. 52 (2009) 42.
[14] S.T. Oyama, T. Gott, H. Zhao, Y.-K. Lee, Catal. Today 143 (2009) 94.
[15] A.F. Gaudette, A.W. Burns, J.R. Hayes, M.C. Smith, T. Seda, M.E. Bussell, J. Catal. 272 (2010) 18.
[16] C.M. Sweeney, K.L. Stamm, S.L. Brock, J. Alloys Compd. 448 (2008) 122.
[17] M. Zumbusch, Z. Anorg, Allg. Chem. 243 (1940) 322.
[18] W.P. Rothwell, J.S. Waugh, J.P. Yesinowski, J. Am. Chem. Soc. 102 (1980) 2637.
[19] S.J. Sawhill, D.C. Phillips, M.E. Bussell, J. Catal. 215 (2003) 208.
[20] JCPDS Powder Diffraction File, International Centre for Diffraction Data, Swarthmore, PA, 2000.
[21] C. Stinner, Z. Tang, M. Haouas, T. Weber, R. Prins, J. Catal. 208 (2002) 456.
[22] I. Furo, I. Bakonyi, K. Tompa, E. Zsoldos, I. Heinmaa, M. Alla, E. Lippmaa, J. Phys. Condens. Matter 2 (1990) 4217.
[23] S.J. Sawhill, K.A. Layman, D.R. Van Wyk, M.H. Engelhard, C. Wang, M.E. Bussell, J. Catal. 231 (2005) 300.
[24] A.W. Burns, A.F. Gaudette, M.E. Bussell, J. Catal. 260 (2008) 262.
[25] C.D. Wagner, A.V. Naumkin, A. Kraut-Vass, J.W. Allison, C.J. Powell, J. Rumble, J.R., National Institute of Standards and Technology, July 2010, 2007.
[26] D.C. Phillips, S.J. Sawhill, R. Self, M.E. Bussell, J. Catal. 207 (2002) 266.
[27] J.R. Brenner, C.L. Marshall, R.E. Winans, J. Catal. 166 (1997) 294.
[28] J. Lee, A. Ishihara, F. Dumeignil, E.W. Qian, T. Kabe, J. Mol. Catal. A 213 (2004) 207.
[29] J. Lee, A. Ishihara, F. Dumeignil, K. Miyazaki, Y. Oomori, E.W. Qian, T. Kabe, J. Mol. Catal. A 209 (2004) 155.
[30] M. Egorova, R. Prins, J. Catal. 225 (2004) 417.
[31] W.R.A.M. Robinson, J.N.M. van Gestel, J. Catal. 161 (1996) 539.
[32] S.T. Oyama, X. Wang, Y.-K. Lee, K. Bando, F.G. Requejo, J. Catal. 210 (2002) 207.
[33] S.T. Oyama, X. Wang, F.G. Requejo, T. Sato, Y. Yoshimura, J. Catal. 209 (2002) 1.
[34] X. Wang, P. Clark, S.T. Oyama, J. Catal. 208 (2002) 321.
[35] S.T. Oyama, J. Catal. 216 (2003) 343.
[36] J.A. Rodriguez, J.-Y. Kim, J.C. Hanson, S.J. Sawhill, M.E. Bussell, J. Phys. Chem. B 107 (2003) 6276.
[37] T. Korányi, Appl. Catal. A: Gen. 239 (2003) 253.
[38] S.T. Oyama, X. Wang, Y.-K. Lee, W.-J. Chun, J. Catal. 221 (2004) 263.
[39] K.A. Layman, M.E. Bussell, J. Phys. Chem. B 108 (2004) 10930.
[40] K.A. Layman, M.E. Bussell, J. Phys. Chem. B 108 (2004) 15791.
[41] Y.-K. Lee, S.T. Oyama, J. Catal. 239 (2006) 376.
[42] M. Lu, A. Wang, X. Li, M. Zhang, K. Tao, Energy Fuels 21 (2007) 554.

[43] Y.-K. Lee, Y. Shu, S.T. Oyama, Appl. Catal. A 322 (2007) 191.
[44] I.I. Abu, K.J. Smith, Appl. Catal. A 328 (2007) 58.
[45] T. Koranyi, Z. Vit, C.C. Poduval, R. Ryoo, H.S. Kim, E.J.M. Hensen, J. Catal. 253 (2008) 119.
[46] R. Wang, K.J. Smith, Appl. Catal. A 361 (2009) 18.
[47] Q. Guan, W. Lei, M. Zhang, K. Tao, J. Catal. 263 (2009) 1.
[48] J.A. Cecilia, A. Infantes-Molina, E. Rodriguez-Castellon, A. Jimenez-Lopez, J. Catal. 263 (2009) 4.
[49] J.A. Cecilia, A. Infantes-Molina, E. Rodriguez-Castellon, A. Jimenez-Lopez, J. Phys. Chem. C 113 (2009) 17032.
[50] I.I. Abu, K.J. Smith, J. Catal. 241 (2006) 356.
[51] A.W. Burns, K.A. Layman, D.H. Bale, M.E. Bussell, Appl. Catal. A 343 (2008) 68.
[52] S. Rundqvist, A. Hede, Acta Chem. Scand. 14 (1960) 893.
[53] R.G. Ross, W. Hume-Rothery, J. Less-Common Met. 5 (1963) 258.
[54] I.R. Shein, A.L. Ivanovskii, Russ. J. Inorg. Chem. 48 (2003) 391.
[55] E.L. Muetterties, J.C. Sauer, J. Am. Chem. Soc. 96 (1974) 3410.
[56] S.S. Chuang, S.-I. Pien, C. Sze, J. Catal. 126 (1990) 187.
[57] Y. Shu, Y.-K. Lee, S.T. Oyama, J. Catal. 236 (2005) 112.